Biophysics and Physicobiology

Regular Article

Mathematical model of structural changes in nuclear speckle

Shingo Wakao[1], Noriko Saitoh[2], Akinori Awazu[1,3]

[1] *Graduate School of Integrated Sciences for Life, Hiroshima University, Higashihiroshima, Hiroshima 739-8526, Japan*

[2] *Division of Cancer Biology, The Cancer Institute of Japanese Foundation for Cancer Research, Koto-ku, Tokyo 135-8550, Japan*

[3] *Research Center for the Mathematics on Chromatin Live Dynamics, Hiroshima University, Higashihiroshima, Hiroshima 739-8526, Japan*

Nuclear speckles are nuclear bodies consisting of populations of small and irregularly shaped droplet-like molecular condensates that contain various splicing factors. Recent experiments have revealed the following structural features of nuclear speckles: (I) Each molecular condensate contains SON and SRRM2 proteins, and *MALAT*1 non-coding RNA surrounds these condensates; (II) During normal interphase of the cell cycle in multicellular organisms, these condensates are broadly distributed throughout the nucleus. In contrast, when cell transcription is suppressed, the condensates fuse and form strongly condensed spherical droplets; (III) SON is dispersed spatially in *MALAT1* knocked-down cells and *MALAT1* is dispersed in SON knocked-down cells because of the collapse of the nuclear speckles. However, the detailed interactions among the molecules that are mechanistically responsible for the structural variation remain unknown. In this study, a coarse-grained molecular dynamics model of the nuclear speckle was developed by considering the dynamics of SON, SRRM2, *MALAT1*, and pre-mRNA as representative components of the condensates. The simulations reproduced the structural changes, which were used to predict the interaction network among the representative components of the condensates.

Key words: molecular condensate, nuclear bodies, splicing factors, molecular interaction network

◀ *Significance* ▶

Nuclear speckles are one of the most prevalent nuclear bodies along with other spherical droplet-like nuclear bodies, such as the nucleolus and promyelocytic leukemia body. However, their structural features differ from those of nuclear speckles distributed broadly throughout the interchromatin compartments of the whole nucleus and exhibit cell state-dependent changes in its shape. Moreover, the mechanism underlying such rich structural changes in nuclear speckles remains unclear. The present study proposed the first mathematical model and revealed the representative components and effective interactions among them, contributing to the knowledge on structural features of nuclear speckles.

Corresponding author: Akinori Awazu, Graduate School of Integrated Sciences for Life, Hiroshima University, 1-3-1, Kagami-yama, Higashi-Hiroshima, Hiroshima 739-8526, Japan. ORCID iD: https://orcid.org/0000-0002-0778-021X, e-mail: awa@hiroshima-u.ac.jp

Introduction

Multicellular organisms contain various non-membranous nuclear bodies in the nuclei of the cells. Their dynamics and biophysical properties are intimately linked to physiological activities, such as gene regulation [1,2]. Typical nuclear bodies, such as the nucleolus and promyelocytic leukemia protein (PML) bodies, form a spherical shape during interphase but they change their structures under certain cellular or experimental conditions and in diseased cells [1,3].

Nuclear speckles are one of the major nuclear bodies formed by over a hundred protein species, including various pre-mRNA splicing factors [4-6] and noncoding RNAs, like *MALAT1* [7,8]. Nuclear speckles are populations of small irregularly-shaped droplet-like molecular condensates distributed throughout the nucleus and enriched in the inter-chromosomal compartments [5,9-16]. Transcriptionally active genes are often found at the periphery of the nuclear speckles [11], and their transcripts are associated with or transit through the nuclear speckles [17,18].

Nuclear speckles were originally identified via immunofluorescence using the monoclonal antibody mAb SC35 that was raised against biochemically isolated mammalian spliceosomes [19]. This antibody had been long considered to be based on immunoblots, and that it recognizes a pre-mRNA splicing factor of 35 kDa of SRSF2/SC35, with possible cross-reactivity to other splicing factors harboring repetitive serine and arginine (SR) sequences. A recent study re-characterized mAb SC35, revealing that its main target may be SRRM2 (formally known as SRm300), which is a spliceosome-associated protein [15]. As the antigens remain somewhat elusive, the mAb SC35-recognizing protein candidates were not yet fully identified but labeled as SC35p. This study examines SRRM2 and SRSF2 as candidates of SC35p.

Recent studies involving high-resolution fluorescence imaging reported the following structural features in nuclear speckles: 1) During interphase, the core region of each small molecular condensate of nuclear speckle contained SON and SC35p, and *MALAT1* tended to surround them like a shell (Figure 1A) [20]; 2) When all gene transcriptions were suppressed, the molecular condensates fused with each other and formed dense spherical condensates with stronger fluorescent intensity than that of the condensates in normal interphase (Figure 1B) [13,20-22]; 3) Conversely, when *MALAT1* was knocked-down, SC35p was sustained in the condensates but SON dispersed (Figure 1C) [20]; IV) Similarly, when SON was knocked-down, SC35p was sustained in the condensates but *MALAT1* dispersed (Figure 1D) [8,20,21]. In the latter two cases, the nuclear speckles were collapsed.
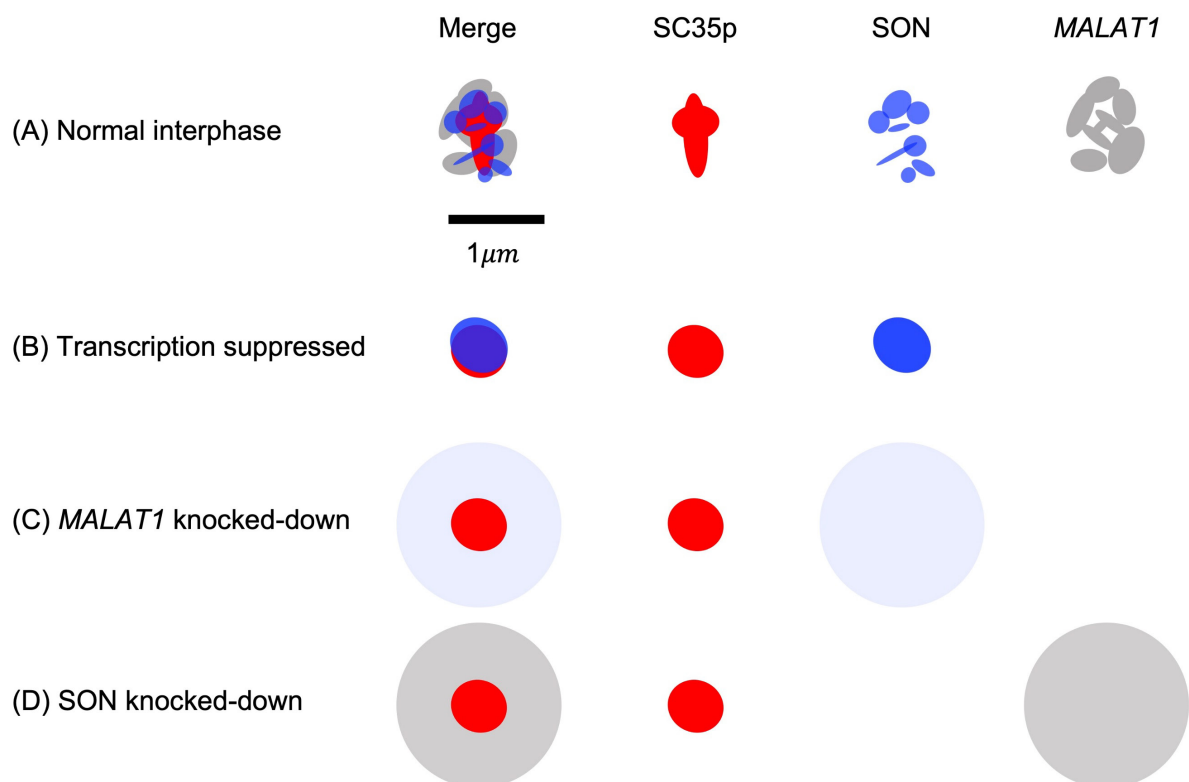

Figure 1 Illustrations of molecular distributions in the nuclear speckle observed using fluorescence microscopy imaging under various conditions. Distribution of SC35p, SON, and *MALAT1* particles during (A) normal interphase [20], (B) transcriptional repression state (Refer to Supplementary Figure S2 in [20] and Figure 7 in [21]), (C) *MALAT1* knocked-down state (Refer to Figure 5 [20]), and (D) SON knocked-down state (Refer to Figure 4 in [20]).

The representative molecules that regulate the structure of nuclear speckles were identified via the aforementioned experiments. However, the detailed interactions among these molecules, which could reveal the underlying mechanisms pertaining to the regulation of the nuclear speckle structure, remain unclear. For other nuclear bodies, such as the nucleolus and paraspeckle, the development of mathematical models have provided deeper insights into the relationships between their structural behaviors and molecular chemo-mechanical features [3,23,24]. Recently, a mathematical model was developed to explain the molecular condensates of nuclear speckles, and it accounted for the interactions among SON, SC35p, and *MALAT1* and reproduced their hierarchical condensations [20]. However, this model had some flaws. For example, it expected that the dispersion of SON by *MALAT1* knockdown could not be reproduced because this model assumed the presence of SON–SON and SON–SC35p attractive forces.

The aim of this study was to elucidate the mechanism and role played by each molecule of the nuclear speckle in determining its structural features. For this purpose, we first developed a coarse-grained molecular dynamics model consisting of the model particles that were considered the representative components of each droplet-like molecular condensate of the nuclear speckles, namely SON, SC35p, *MALAT1,* and pre-mRNA. Based on recent experiments and simulations of various models with various assumptions regarding the effective interactions among these molecules, we tried to infer the interaction network among the mentioned representative components that could reproduce all the structural changes in each nuclear speckle.

Materials and Methods

Candidates of Proteins Probed with mAb SC35 (SC35p): SRSF2 and SRRM2

mAb SC35 has been used to observe nuclear speckles as this antibody recognizes SRSF2/SC35. However, a recent re-characterization study revealed that a major target for this antibody may actually be SRRM2 [15]. Therefore, in this study, both SRSF2 and SRRM2 were assumed as SC35p in their individual models. The model assuming SC35p as SRSF2 was named the SF2 model and that assuming SC35p as SRRM2 was named the RM2 model.

Coarse-Grained Models of SON, SRRM2, and SRSF2

All three selected proteins, SON, SRRM2, and SRSF2, are intrinsically disordered proteins that involve partially folded regions, and their intrinsically disordered regions (IDRs) occupy a large ratio of their amino acid sequences (Figure 2A, B) [4,25,26]. This indicates that they do not possess unique stable folding structures but change their shapes like random polymers. Therefore, each of these proteins was described using one soft spherical particle with their respective radii r^p (p : SON, SRRM2, SRSF2) for simplicity. Here, the particles representing SON, SRRM2, and SRSF2 were named the SON, SRSF2, and SRRM2 particle, respectively. Each particle indicates the spatial region that the chain tends to occupy on the protein. Therefore, the excluded volume effects among these particles were assumed to be weak enough that a significant portion of the regions in the two contacting particles was allowed to overlap with each other (Supplementary Figure S1).

The radii r^p were assumed according to the arguments of random polymers with excluded volume as $r^p = [\mathrm{ACd}]\left(\frac{L^p}{[\mathrm{ACd}]}\right)^{\frac{3}{5}}$, where $[\mathrm{ACd}] = 0.36$ nm indicates the average distance between the edge of the amino group and that of the carboxyl group in each amino acid and L^p indicates the effective protein length. In the present study, for the SON and SRSF2 models, L^p was defined as the edge-to-edge distance of proteins containing secondary structures along the amino acid sequence as follows: $L^p =$ [sum of all distances between N-terminals and C-terminals of partially folded regions (nm)] + [ACd]·[Number of amino acids belonging to IDR] (Figure 2A, B, Supplementary Figure S2). The three-dimensional coordinates of atoms and positions of folded regions in SON and SRSF2 were obtained in PDB format files from the UniProt database [https://www.uniprot.org] ID Q01130 and P18583 [27], where these features were inferred using Alpha-Fold2 [28,29]. Based on these estimates, $r^{\mathrm{SON}} = \sim 18.4$ nm and $r^{\mathrm{SRSF2}} = \sim 3.4$ nm were obtained.

In this study, SRRM2 was assumed to be a simple unfolded random polymer of amino acids because most of the regions were IDRs, and no public data of the three-dimensional coordinates of the atoms and positions of folded regions in SRRM2 were available (Figure 2C). Therefore, $L^p = [\mathrm{ACd}]$·[Number of amino acids belonging to IDR] was assumed, which yielded the value $r^{\mathrm{SRRM2}} = \sim 20.8$ nm.

The molecules of focus in this study were expected to be more rigid in their central regions than random polymers would be but similar to them in their outer regions. The rigidity of a random polymer with excluded volume decreases with an increase in the number of segments corresponding to $\frac{L^p}{[\mathrm{ACd}]}$ but theoretical basis for the exact formulation of L^p and [ACd] dependency of such rigidity remains known. However, recent molecular dynamics simulations showed that the elastic stress–strain relations of random polymers with excluded volumes could be approximated using those of ideal chains when the polymer concentrations were not as high as those of solids [30]. Therefore, in this model, the rigidity parameters of these particles, q^p, were assumed to be proportional to the estimated conventional arguments of the rubber

elasticity of ideal chains, as follows: $q^p = \frac{k_BT}{L^p[\text{ACd}]}$. Here, $q^{\text{SON}} = \sim 1.43 \times 10^{-5}\,\text{kg}\cdot\text{s}^{-2}$, $q^{\text{SRRM2}} = \sim 1.16 \times 10^{-5}\,\text{kg}\cdot\text{s}^{-2}$, and $q^{\text{SRSF2}} = \sim 2.35 \times 10^{-4}\,\text{kg}\cdot\text{s}^{-2}$ were obtained.
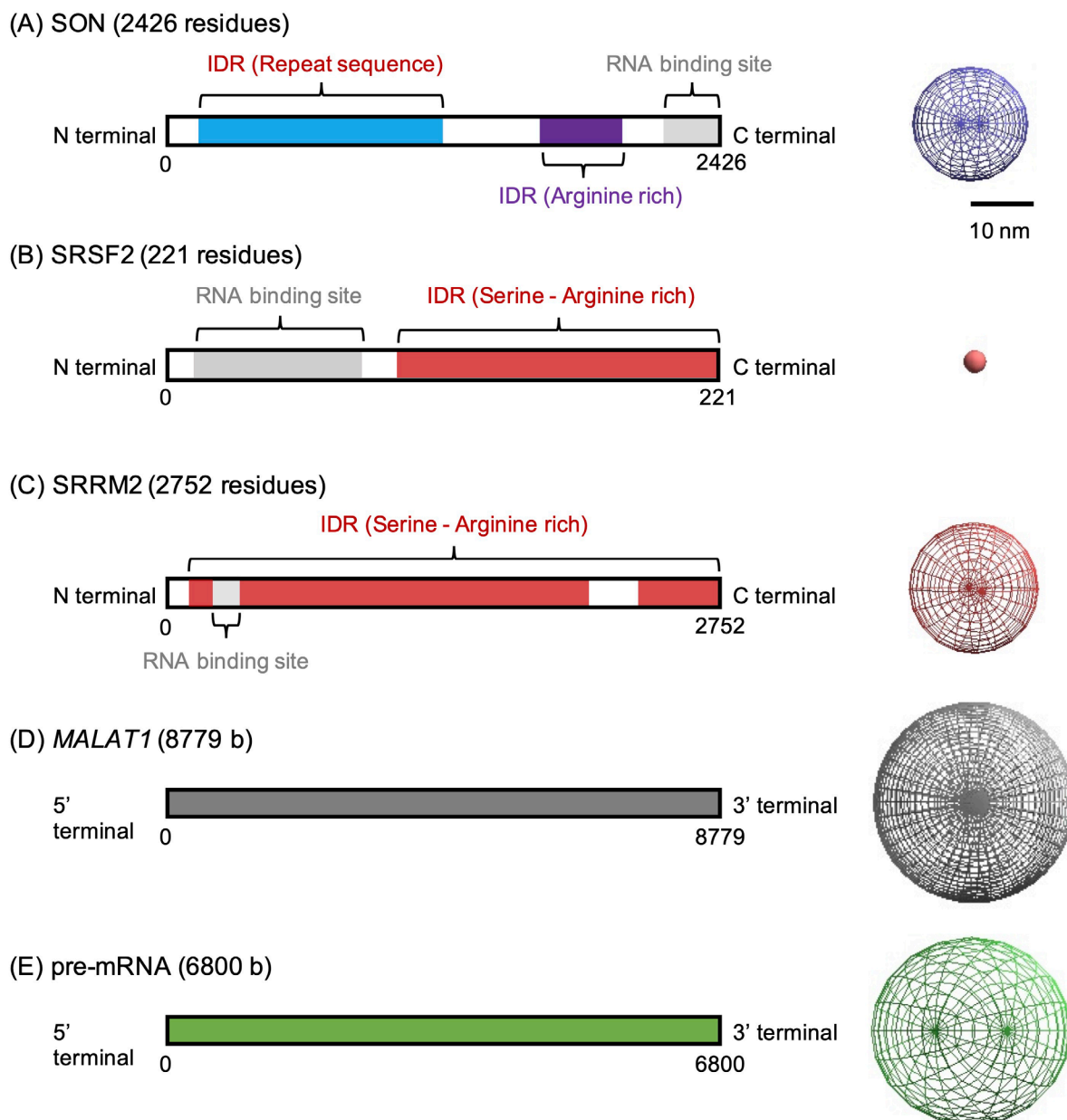

Figure 2 Construction of a coarse-grained model of each molecule. Lengths and local regions in proteins and RNAs (left) and soft spherical particle models (right) of (A) SON, (B) SRSF2, (C) SRRM2, (D) *MALAT1*, and (E) pre-mRNA. IDR, intrinsically disordered region.

Coarse-Grained Models of *MALAT1* and Pre-mRNAs

In the present model, RNAs were assumed to be unfolded random polymers, and each RNA chain was described as one soft spherical particle with their respective radii r^R (R : *MALAT1* or pre-mRNA). Here, the particles representing *MALAT1* and pre-mRNA were respectively called *MALAT1* and pre-mRNA particles. Similar to protein models, each particle indicated the spatial region that the chain tended to occupy on the protein (Figure 2D, E); therefore, the excluded volume effects among these particles were assumed to be weak enough that a small portion of the regions in the two contacting particles were allowed to overlap with each other.

The radii r^R were assumed as $r^p = [5' - 3' \text{distance}][\text{number of nucleotides}]^{\frac{3}{5}}$, where $[5' - 3' \text{distance}]$ was assumed as 0.3 nm and the number of nucleotides for *MALAT1* was assumed as 8779 bp. In the present study, the number of pre-mRNAs was assumed to be a unique value of 6.8 kb, which was the same value as that of the average base pairs of gene-transcribed regions in the human genome; this was estimated based on the Refseq data [31]. The rigidity parameters of these particles, q^R, were also estimated in a similar way, where $q^R = \frac{k_B \text{T}}{[\text{number of nucleotides}][5'-3'\text{distance}]^2}$ was assumed. Further the values $r^{MALAT1} = \sim 33.0$ nm, $r^{\text{pre}-\text{mRNA}} = \sim 29.9$ nm, $q^{MALAT1} = \sim 5.75 \times 10^{-6}$ kg · s^{-2}, and $q^{\text{pre}-\text{mRNA}} = \sim 6.76 \times 10^{-6}$ kg · s^{-2} were obtained.

Motion of Each Molecule

As each biomolecule was expected to exhibit three-dimensional Brownian motion in the nucleus, the position of the i-th particle with radius r_i in the (x, y, z) three-dimensional space $\boldsymbol{x}_i = (x_i, y_i, z_i)$ was assumed to obey the Langevin equation as follows:

$$\gamma_i \frac{dx_i}{dt} = -\frac{\partial}{\partial x_i} V + \boldsymbol{R}_i(t) \tag{1}$$

where γ_i and $\boldsymbol{R}_i(t)$ are the coefficients of drag force and Gaussian white noise, respectively, playing the role of the random force from the nucleoplasm to i-th particle and obeying $\langle \boldsymbol{R}_i(t) \rangle = 0$ and $\langle \boldsymbol{R}_i(t) \boldsymbol{R}_{i'}(s) \rangle = 6\gamma_i k_B T \delta_{i\,i'} \delta(t - s)$ with Boltzmann constant k_B and temperature T, where $k_B T = 4.141947 \times 10^{-21}$ kg m^2 s^{-2} ($T = 300$ K). Here, δ_{ij} indicates the Kronecker delta, and $\delta(\ldots)$ indicates the Dirac delta function. The term V indicates that the potential of the system involves the potential of forces among the particles and effect of the boundary conditions. The drag coefficient γ_i for each particle was assumed as $6\pi\eta r_i$, with the viscosity of the nucleoplasm $\eta = 0.64$ kg m^{-1} s^{-1} [32].

Particle motion was assumed to be restricted to a spherical region with a radius of 500 nm. although 500 nm was slightly larger than the characteristic length of the inter-chromosomal components in the cell's nucleus. A wider space was employed in the simulations to infer the mechanism underlying the droplet structures from the self-assembling behaviors of nuclear speckle components without the influence of other factors such as chromatin territories and other nuclear bodies.

Model of Effective Interactions among Molecules

The potential of system V to provide the forces working on and among the particles is given as:

$$V = V_{collision} + V_{attract} + V_{boundary} \tag{2}$$

where $V_{collision}$ is the potential of the collisional interactions among the particles owing to their excluded volumes, $V_{attract}$ is the potential of the attractive interactions among the particles owing to the electrostatic interactions or biochemically specific affinities among molecules, and $V_{boundary}$ is the potential of the effect of the boundary wall to restrict particles in the above-mentioned spherical region.

The potential V_{col} was calculated using the following equation:

$$V_{collision} = \sum_{i<i'} \theta\big((r_i + r_{i'}) - |\boldsymbol{x}_i - \boldsymbol{x}_{i'}|\big) C_{i,i'} k_{i,i'}^c \left[-2 \left(\frac{r_i + r_{i'}}{|x_i - x_{i'}|} \right)^6 + \left(\frac{r_i + r_{i'}}{|x_i - x_{i'}|} \right)^{12} + 1 \right] \tag{3}$$

where $k_{i,i'}^c = k_0^c \sqrt{q_i q_{i'}}$ represents the repulsion strength, and $C_{i,i'} = 1\ or\ 0$ when repulsion works or does not work, respectively, in between the i-th and i'-th particles.

θ is the Heaviside step function and is defined as follows:

$$\theta(y) = \begin{cases} 1\ (y \geq 0) \\ 0\ (y < 0) \end{cases} \tag{4}$$

The potential $V_{attract}$ was calculated based on the equation:

$$V_{attract} = \sum_{i<i'} A_{i,i'} k_{i,i'}^a \left[-2 \left(\frac{(r_i + r_{i'}) - d_{i,i'}}{|x_i - x_{i'}|} \right)^6 + \left(\frac{(r_i + r_{i'}) - d_{i,i'}}{|x_i - x_{i'}|} \right)^{12} \right] \tag{5}$$

where $k_{i,i'}^a$ represents the strength of the attractive force, and the value of $A_{i,i'}$ is 1 or 0 when the attractive force works

or does not work, respectively, in between the i-th and i'-th particles. $d_{i,i'}$ was assumed to be smaller than $r_i + r_{i'}$ because the particles representing the space occupied by polymers were assumed to be soft enough that the stable distance between the two particles was expected to be nearer than the sum of their radii when attractive forces worked in between them. In this study, $d_{i,i'}$ was chosen to satisfy the following relation:

$$\theta\left((r_i + r_{i'}) - d_{i,i'}\right) k_{i,i'}^c \left[-2\left(\frac{r_i+r_{i'}}{(r_i+r_{i'})-d_{i,i'}}\right)^6 + \left(\frac{r_i+r_{i'}}{(r_i+r_{i'})-d_{i,i'}}\right)^{12} + 1\right] = \frac{k_B T}{2} \tag{6}$$

where $d_{i,i'}$ provided the typical length of the region where two particles could overlap when only the repulsion represented by Eq. (3) was assumed to work in between them (Supplementary Figure S1).
The potential $V_{boundary}$ was calculated based on the following equation:

$$V_{boundary} = \sum_{i<i'} \theta\left((R - r_i) - |\boldsymbol{x}_i|\right) k^w q_i \left[-2\left(\frac{R-r_i}{|\boldsymbol{x}_i|}\right)^6 + \left(\frac{R-r_i}{|\boldsymbol{x}_i|}\right)^{12} + 1\right] \tag{7}$$

where k^w represents the strength of the restriction from the boundary wall, and R represents the radius of the simulation space (assumed as 500 nm).
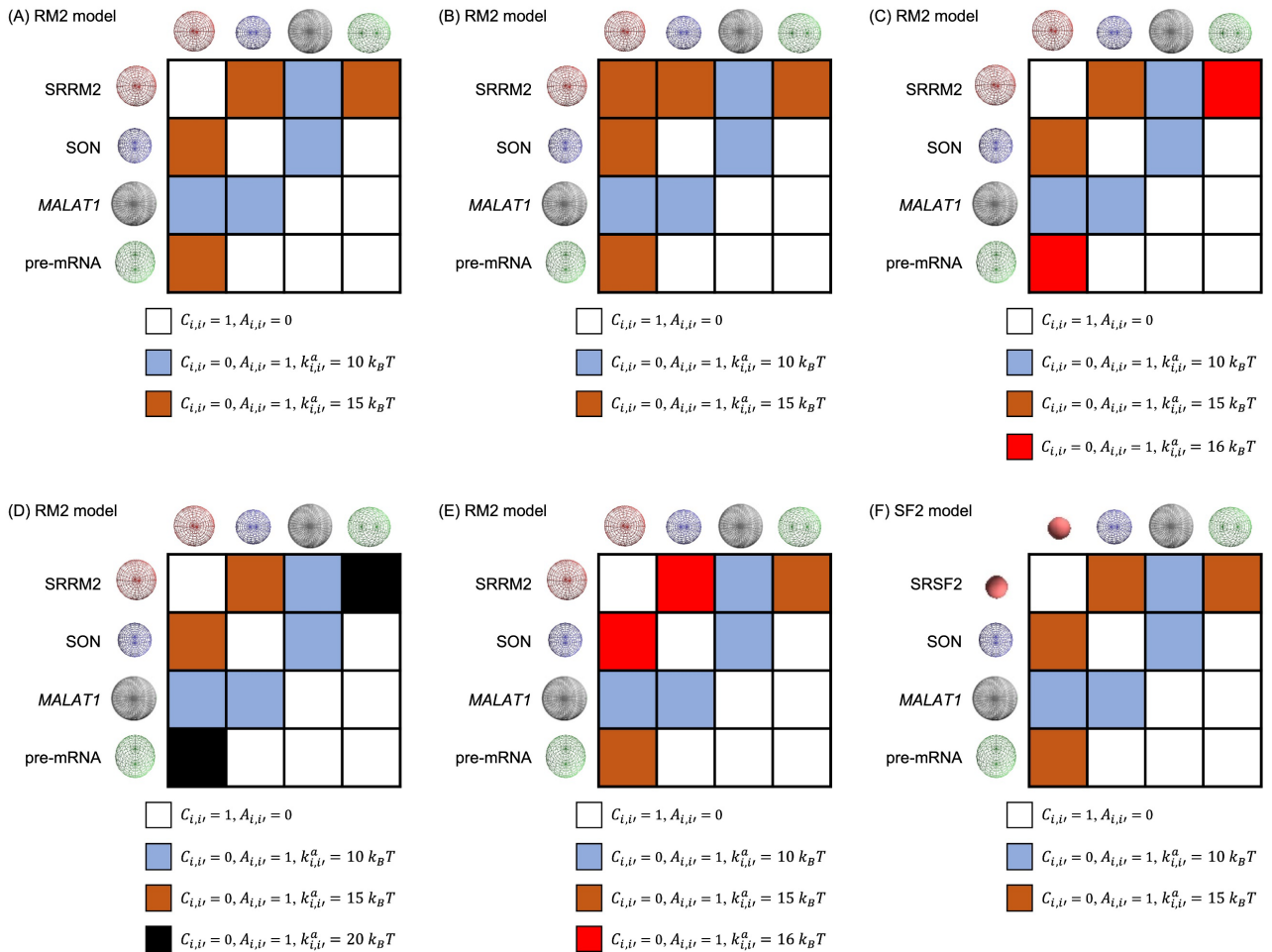

Figure 3 Matrices of the considered interaction networks among the particles in RM2 (A-E) and SF2 (F) models. White boxes indicate repulsion, blue, brown, red, and black boxes indicate attraction between a pair of particles. Each profile of interaction potential between each pair of particles in (A) is shown as an example in Supplementary Figure S1.
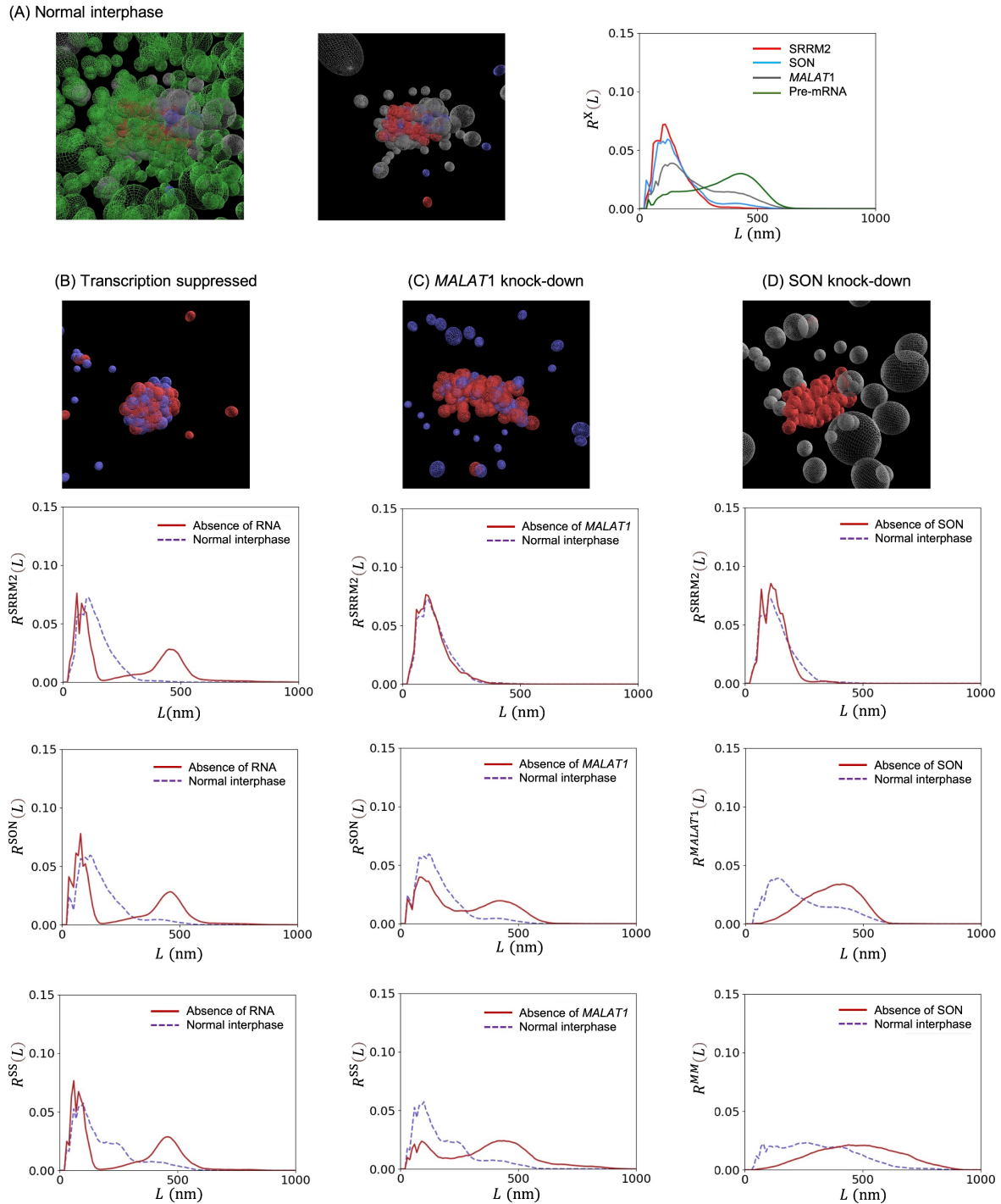
Figure 4 Simulation results of the RM2 model with appropriately designed parameters. (A) Typical snapshots of the simulations (left), the same snapshots without showing the pre-mRNA particles (middle), and radial distributions of particles, $R^{\mathrm{SRRM2}}(L)$, $R^{\mathrm{SON}}(L)$, $R^{MALAT1}(L)$, and $R^{\mathrm{pre-mRNA}}(L)$ (right) in the case of normal interphase. (B–D) Typical snapshots of the simulations (pre-mRNA particles are not shown) (first), $R^{\mathrm{SRRM2}}(L)$ (second), $R^{\mathrm{SON}}(L)$ or $R^{MALAT1}(L)$ (third), and $R^{\mathrm{SON}}(L)$ or $R^{MALAT1}(L)$ and $R^{\mathrm{SS}}(L)$ or $R^{MM}(L)$ (fourth) in the case where (B) transcription was suppressed, (C) *MALAT1* was knocked-down, and (D) SON was knocked-down. Each particle color indicates a different molecular species as explained in Figure 2. SRRM2 particles tended to distribute at the central region of the simulation space indicated by the spherical region with radius = 500 nm (Supplementary Figure S4). Thus, peaks of $R^{\mathrm{SRRM2}}(L)$, $R^{\mathrm{SON}}(L)$, $R^{MALAT1}(L)$, and $R^{\mathrm{pre-mRNA}}(L)$ with L sufficiently smaller than 500 nm were expected to show boundary-independent particle concentration features around SRRM2 particles.

Simulation and Data Analysis Method

The time integral of Langevin Eq. (1) was calculated numerically using the Eular–Maruyama method with a unit step of 3.16×10^{-7} s. For the initial condition (time = 0 s), the particles were placed randomly in the sphere within a radius of $250\ nm$. The radial distributions of distances between two particles are defined as $R^{X,Y}(L) = $ [Probability that the distance between X and Y particles = $L\ and\ L + \Delta$]. Notably, the accumulation or dispersion features of the X and Y particle populations, in particular the position, height, and width of the first peak nearest from $dist = 0$ of $R^{X,Y}(L)$, were provided by the profile.

Recent experimental studies suggested that SC35p always formed condensates independent of the cell state [8,13,20-22]. Therefore, to evaluate the structural features of particle condensates, the radial distributions of SC35p (SRRM2 or SRSF2), SON, *MALAT1*, and pre-mRNA particles from SC35p (SRRM2 or SRSF2) particles were measured; the radial distribution of X particle (X = SON, SRSF2, SRRM2, *MALAT1*, or pre-mRNA) was defined as $R^{X}(L) = $ [Probability that the distance between X and SC35p (SRRM2 or SRSF2) particles was given between $L\ and\ L + \Delta$]. Here, the bin of $R^{X}(L)$ was given as $\Delta = 10$nm. Additionally, the radial distributions of SON particles from other SON particles and those of *MALAT1* particles from other *MALAT1* particles are defined as $R^{SS}(L) = $ [Probability that the distance between a SON and other SON particles was given between $L\ and\ L + \Delta$] and $R^{MM}(L) = $ [Probability that the distance between a *MALAT1* and other *MALAT1* particles was given between $L\ and\ L + \Delta$], respectively, which were also measured to evaluate their condensations or dispersions. These distributions were estimated using the particle configurations between the time interval $403 - 474\ s$, where the radial distribution of the typical state was obtained without the influence of the initial particle configuration.

Additionally, if particles distribute uniformly, the radial distribution generally exhibits an increase in L that is proportion to L^2. Due to the restriction of boundary conditions, however, the radial distribution starts to decrease in L around $L = 400 - 500$ nm when the particles were confined in the spherical space of radius = 500 nm. Therefore, the emergence of a gradual peak around $L = 400 - 500$ nm in the radial distribution means that the particles did not exhibit any specific localizations but distributed almost uniformly (Supplementary Figure S3). Conversely, the peak near $L = 0\ nm$ indicated the features of specific localizations of particles.

Results

Constraints on Estimation of Interaction Network from Experimental Facts and Biochemical Properties of Molecules

The aim of this study was to identify the effective interaction network among the representative molecules forming each droplet-like condensate of nuclear speckles. Based on the inconsistencies between the preliminary considered model and the observed experimental facts, we deduced that the effective molecular interactions among these molecules seemed to obey the following constraints (Figure 1) [8,13,20-22].

First, an attractive force between SON and pre-mRNA cannot be assumed because the model with such an interaction cannot reproduce the dispersion of SON in the scenario of *MALAT1* knock-down (Figure 1C) (explained later). For the same reason, neither can a self-attractive force be assumed between SONs.

Second, an attractive force between *MALAT1* and pre-mRNA cannot be assumed because the model with such an interaction cannot reproduce the dispersion of *MALAT1* in the SON knock-down scenario (Figure 1D). The repulsion between *MALAT1* and pre-mRNA was also supported by their electrostatic properties; both RNAs involve negative charge. For the same reason, neither can a self-attractive force be assumed between *MALAT1* and pre-mRNA.

Third, an attractive force between SC35p and *MALAT1* was weaker than that between SC35p and SON because SON tends to locate close to SC35p, and *MALAT1* tends to surround SON–SC35p condensate during normal interphase (Figure 1A).

Additionally, the dissociation energies between two attractive interacting molecules that provide the strength between these molecules ($k_{i,i'}^{a}$) were assumed as $k_{i,i'}^{a} = 10 - 20\ k_{B}T$. This assumption indicated that the binding between the molecules was sufficiently strong against thermal fluctuations but could be dissociated in the reaction process with ATP hydrolysis.

Simulation of the RM2 Model Using Specific Molecular Interactions Reproducing Condensation and Dispersion of Molecules in Nuclear Speckles

The RM2 model was developed with the following specific intermolecular interactions based on the arguments presented in the previous section (Figure 3A, Supplementary Figure S1):

I) Repulsive forces caused by the excluded volumes of molecules between two particles representing the same molecular species were assumed as $C_{i,i'} = 1$ and $A_{i,i'} = 0$. The parameter providing the strength of the repulsive forces, k_{0}^{c}, was given as $1.4 \times 10^3\ k_{B}T$.

II)   A specific attractive force between SRRM2 and SON particles and between SRRM2 and pre-mRNA particles was assumed as $C_{i,i\prime} = 0$ and $A_{i,i\prime} = 1$. The attractive strength parameter was assumed uniformly as $k_{i,i\prime}^a = 15\ k_B T$.

III)   A specific attractive force between SRRM2 and *MALAT1* particles and between SON and *MALAT1* particles was assumed as $C_{i,i\prime} = 0$ and $A_{i,i\prime} = 1$. The attractive strength parameter was assumed uniformly as $k_{i,i\prime}^a = 10\ k_B T$.

IV)   The interactions between SON and pre-mRNA particles and that between *MALAT1* and pre-mRNA particles were assumed to be repulsive, as $C_{i,i\prime} = 1$, $A_{i,i\prime} = 0$, and $k_0^c = 1.4 \times 10^3\ k_B T$.

Simulations of this model were able to reproduce the experimentally observed structural features of the nuclear speckle droplets (Figure 1) as follows:

First, the number of SRRM2, SON, *MALAT1*, and pre-mRNA particles were assumed to be 60, 60, 60, and 420, respectively, and they were simulated to consider the behavior of nuclear speckle droplets under normal conditions during interphase. The present model exhibited broadly distributed particle condensates (Figure 4A). Further, $R^{SON}(L)$, $R^{SRRM2}(L)$, and $R^{MALAT1}(L)$ exhibited peaks at a similar L near $L = 0$ but $R^{MALAT1}(L)$ involved a lower peak. Conversely, $R^{MALAT1}(L)$ exhibited larger value than did $R^{SON}(L)$ and $R^{SRRM2}(L)$ at the region far from $dist = 0$. This indicates that the condensates of SRSF2 and SON particles were surrounded by *MALAT1* particles similar to the core–shell structure observed in the experiments (Figure 1A) [14,20].

Second, to consider the scenario of suppression of transcription activity in the entire nucleus, the number of SRRM2, SON, *MALAT1*, and pre-mRNA particles were assumed as 60, 60, 0, and 0, respectively. The positions of the large peaks that were nearest from $L = 0$ of $R^{SRRM2}(L)$, $R^{SON}(L)$, and $R^{SS}(L)$ had shifted closer to $L = 0$, and their widths became smaller than that in the previous case (Figure 4B). This indicates that SRRM2 and SON had formed a denser condensate than that in the previous case, and the formation of denser droplets observed in the experiments can be attributed to transcription suppression (Figure 1B) [13,21,22].

Third, to consider the *MALAT1* knocked-down state, the number of SRRM2, SON, *MALAT1*, and pre-mRNA particles were assumed to be 60, 60, 0, and 420, respectively. In this case, the qualitative features of $R^{SRSF2}(L)$ were almost unchanged from that in the first case. However, $R^{SON}(L)$ and $R^{SS}(L)$ were broader, and the peak nearest to $L = 0$ was much smaller than that in the first case (Figure 4C). This indicates that SON was spatially dispersed as observed in *MALAT1* knockdown experiments (Figure 1C) [20].

Finally, to consider the SON knocked-down state, the number of SRRM2, SON, *MALAT1*, and pre-mRNA particles were assumed as 60, 0, 60, and 420, respectively. In this case, the qualitative features of $R^{SRSF2}(L)$ were almost unchanged from that in the first case. However, $R^{MALAT1}(L)$ and $R^{MM}(L)$ were broader, and the peak nearest to $dist = 0$ was much smaller than that in the first case (Figure 4D). This indicates that *MALAT1* was spatially dispersed, as observed in the SON knockdown experiments (Figure 1D) [8,20,21].

Notably, this model did not involve the self-attractive force between SC35p particles because of its simplicity; however, this attractive force could be assumed according to the arguments put forth in the previous section. Nevertheless, the results were qualitatively unchanged even when the self-attractive force between the SC35p particles was assumed to be similar in strength as that between SC35p and SON particles. This can be confirmed by simulating the scenario where the specific self-attractive force between SRRM2 particles was assumed as $C_{i,i\prime} = 0$, $A_{i,i\prime} = 1$, and $k_{i,i\prime}^a = 15\ k_B T$ in addition to the interactions described in specifications I)–IV) (Figure 3B, Supplementary Figure S5).

## Molecular Interaction Parameters-dependent Behaviors of RM2 Model

The RM2 model simulated based on the interactions assumed in specifications I)–IV) in the previous section exhibited behaviors consistent with all observed experimental phenomena (Figure 1 and Figure 4). The strength of the attractive force between SRRM2 and pre-mRNA particles was assumed to be the similar to that between SRRM2 and SON particles. The attractive force between SRRM2 and *MALAT1* was expected to be weaker than that between SRRM2 and SON particles, consistent with previous considerations. However, the appropriate interaction strength between SRRM2 and pre-mRNA could not be determined based on these considerations alone. Therefore, further RM2 model simulations were performed with attractive forces between SRRM2 and pre-mRNA particles that were stronger or weaker than that between SRRM2 and SON particles.

For examples, the coefficient of the attractive force between SRRM2 and pre-mRNA particles was assumed as $k_{i,i\prime}^a = 16\ k_B T$ and $k_{i,i\prime}^a = 20\ k_B T$, whereas the coefficient of the attractive force between SRRM2 and SON particles was assumed as $k_{i,i\prime}^a = 16\ k_B T$. The interaction strengths among all other particles were assumed to be the same as those mentioned in specifications I)–IV) presented in the previous section.

In the case where $k_{i,i\prime}^a = 16\ k_B T$ was assumed to be the attractive force between SRRM2 and pre-mRNA particles (Figure 3C), the simulation exhibited the same qualitative results as those obtained for the simulations of previously considered RM2 models (Supplementary Figure S6). However, when the attractive force between SRRM2 and pre-

mRNA particles becomes sufficiently larger than that between SRRM2 and SON particles, for example, in the case where $k_{i,i'}^a = 20\ k_B T$ (Figure 3D), the particles tend to be divided into SRRM2 particle condensates and SON–*MALAT1* particle condensates, and SRRM2 particles tend to be surrounded by pre-mRNA particles (Figure 5A). Conversely, in the case where $k_{i,i'}^a = 16\ k_B T$, and the attractive force between SRRM2 and SON particles was slightly stronger than that between SRRM2 and pre-mRNA particles (Figure 3E), and the condensate of SRRM2, SON, and *MALAT1* particles were similar to that obtained in the case of normal interphase (as explained in the previous section). However, in such cases, the dispersion of SON was weakened and SON tended to locate near SRRM2 even in the case of *MALAT1* knock-down (Figure 5B).

(A) Normal interphase: [SRRM2 - pre-mRNA attraction] >> [SRRM2 – SON attraction]
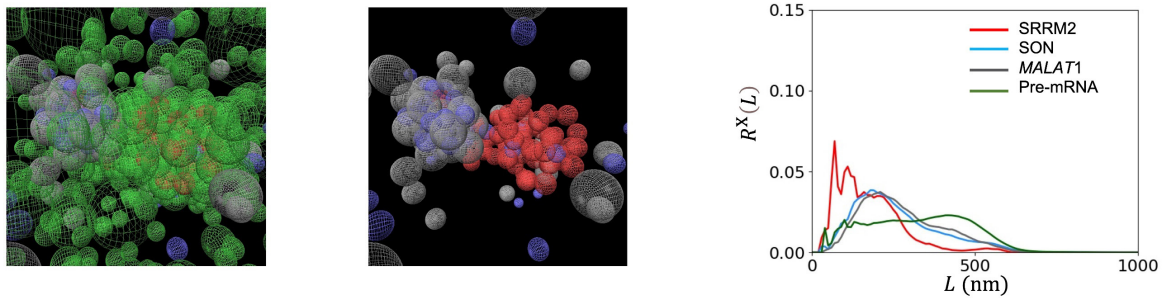
(B) *MALAT1* knock-down : [SRRM2 - pre-mRNA attraction] < [SRRM2 – SON attraction]
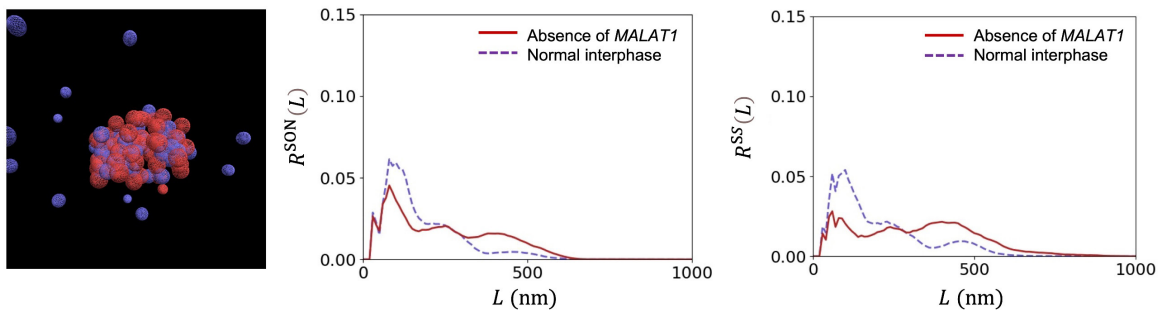

Figure 5 Results of the RM2 model simulation where the attractive force between SRRM2 and pre-mRNA particles was assumed to be stronger or weaker than that between SRRM2 and SON particles. (A) Typical snapshots of the simulations (left), the same snapshots without showing the pre-mRNA particles (middle), and radial distributions of particles, $R^{\mathrm{SRRM2}}(L)$, $R^{\mathrm{SON}}(L)$, $R^{MALAT1}(L)$, and $R^{\mathrm{pre-mRNA}}(L)$ (right) in the scenario of normal interphase when the attractive force between SRRM2 and pre-mRNA particles was stronger than that between SRRM2 and SON particles. (B) Typical snapshots of the simulations (pre-mRNA particles are not shown) (left), $R^{\mathrm{SON}}(L)$ (middle), and $R^{\mathrm{SS}}(L)$ (right) in the scenario of *MALAT1* knock-down and weaker attractive force between SRRM2 and pre-mRNA particles than that between SRRM2 and SON particles. Each particle color indicates the respective molecular species explained in Figure 2. The results seemed to be qualitatively the same as those obtained in Figure 4.

Inferred Result of Molecular Interaction Network Using RM2 Model

The simulation results presented in the two previous sections suggest that the following roles are played by the representative molecules and the following mechanism are the cell state-dependent features of each molecular condensate comprising the nuclear speckles (Figure 6):

A) SRRM2 exhibited attractive interactions with all other representative nuclear speckle component molecules; SRRM2–SON interaction was assumed to be similar (Figure 3–4) or slightly weaker than the SRRM2–pre-mRNA interaction (Supplementary Figure S4); SRRM2–MALAT1 interaction was assumed to be slightly weaker than the SRRM2–SON interaction (Figure 6A); attractive interactions also occurred between SON and *MALAT1*.

B) During normal interphase in the cell's nucleus, the pre-mRNAs and SON–*MALAT1* complexes are considered to cluster around SRRM2. However, they were expected to spread spatially owing to their mutual repulsive forces. Notably, the attractive interaction between SRRM2 and SON or *MALAT1* was similar or slightly weaker than that between SRRM2 and pre-mRNA. However, to dissociate from the SON–MALAT1 complex, SRRM2 must dissociate from SON and MALAT1 almost simultaneously; therefore, the attractive

interaction between SRRM2 and SON–MALAT1 complex could be more effective than that between SRRM2 and pre-mRNA (Figure 6A). Hence, SRRM2 distributed to connect with them, which is why the nuclear speckle component was broadly distributed (Figure 6). In such a broad molecular assembly, SON tended to be distributed nearer to *MALAT1* because the attractive force between SON and SRRM2 was stronger than that between SRRM2 and *MALAT1*.

C)   When transcription in the entire nucleus was suppressed, few RNAs existed in the nucleus. Therefore, SON and SRRM2 formed larger dense condensates owing to the mutual attractive interaction between them without competition between SON and pre-mRNA (Figure 6).

D)   When *MALAT1* was knocked down, SON and pre-mRNA competed for binding with SRRM2. However, more pre-mRNA particles could bind to SRRM2 than could SON particles even if the affinity of SON to SRRM2 was similar or slightly weaker than that of pre-mRNA. This is because the volume fraction of pre-mRNA was much larger than that of SON; hence, SRRM2 tended to interact with pre-mRNA more frequently than did SON. The results showed that most of the SRRM2 particles were bound to pre-mRNA particles, whereas SON was excluded; therefore, SRRM2 sustained its condensate but SON dispersed spatially. Similarly, SRRM2 sustained its condensate, but *MALAT1* dispersed spatially when SON was knocked down (Figure 6).
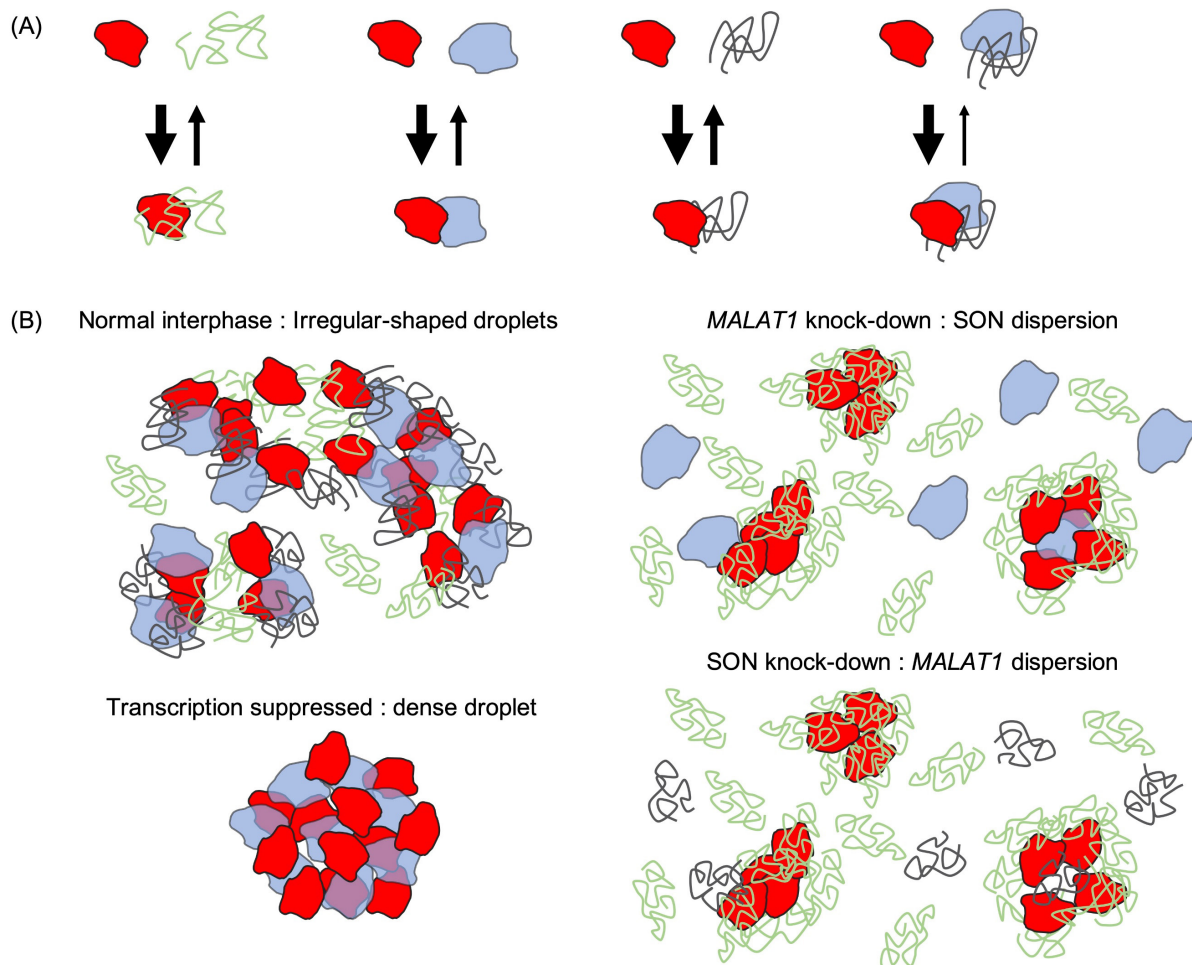

Figure 6 (A) Illustrations of the affinities among SON (blue), SRRM2 (red), MALAT1 (black), and pre-mRNA (green). (B) Mechanism and molecular roles of structural changes in molecular accumulations in nuclear speckles (B). Each color indicates a different molecular species as explained in Figure 2, and arrow width represents transition rates.

Simulation of SF2 Model Using Specific Molecular Interactions

A recent study suggested that a major target for mAb SC35 was SRRM2 [15]. However, SRSF2 could remain a possible target of mAb SC35. Therefore, the SF2 model was also simulated to infer the behaviors in the scenario in which SC35p is SRSF2.

The simulation of the SF2 model for normal interphase was performed with the following assumptions: the interactions among SRSF2 particle and other particles were assumed to be the same as that among SRRM2 particles and other particles assumed in the previous RM2 model (Figure 3F); additionally, the number of SRSF2 particles was assumed to be twice that of the SON and *MALAT1* particles assumed in the previously proposed mathematical model [20] (where the number of SRSF2, SON, MALAT1, and pre-mRNA particles were assumed as 120, 60, 60, and 420, respectively).

In this case, the particles tend to be divided into SRSF2 particle condensates and SON–*MALAT1* particle condensates, where SRSF2 particles tended to be surrounded by the pre-mRNA particles (Figure 7). Here, the attractive force between SRSF2 and SON was assumed be similar to that between SRSF2 and pre-mRNA. Notably, when the strength of the attractive force between SRSF2 and SON was assumed to be stronger than that between SRSF2 and pre-mRNA, the SRSF2, SON, and MALAT1 particle condensate might be formed in the case of normal interphase. However, in such cases, the dispersion of SON cannot occur in the case of *MALAT1* knock-down as would be expected based on similar assumptions as that made for RM2 model (Figure 5 and Figure 6).
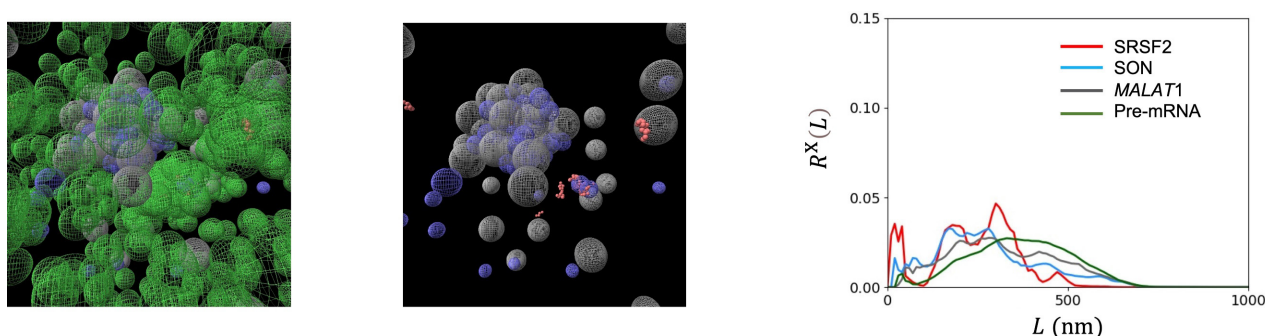

Figure 7 Simulation results of the SF2 model where the parameter for the attractive strength between SRSF2 and *MALAT1* particles and between SON and *MALAT1* particles was modified uniformly to $k_{i,i'}^a = 10\,k_B T$. Matrices of interaction networks among the particles was assumed to be the same as in Figure 3A except that SRRM2 was replaced with SRSF2. Snapshots of the simulations (left), the same snapshots without the pre-mRNA (middle), and radial distributions of the particles $R^{\mathrm{SRSF2}}(L)$, $R^{\mathrm{SON}}(L)$, $R^{MALAT1}(L)$, and $R^{\mathrm{pre-mRNA}}(L)$ (right) in the case of normal interphase. Each particle color indicates a different molecular species as explained in Figure 2.

Discussion

In this study, a coarse-grained molecular dynamics model was developed using SON, SC35p (SRRM2 or SRSF2), *MALAT1*, and pre-mRNA as the representative components of condensates to simulate the structural behavior of droplet-like condensates of nuclear speckles. Simulations of the model where SRRM2 was assumed as SC35p reproduced various experimentally observed cell state-dependent droplet structures. Through these simulations, we predicted the effective interactions and their strengths among the representative components of nuclear speckles. Simulations of the model assuming SRSF2 as SC35p were also performed. However, the simulation results exhibited features inconsistent with the experimentally observed phenomena. These facts suggested that SC35 should be SRRM2 rather than SRSF2, supporting a recent proposal [15].

In the present model, RNAs are assumed to be random polymers. However, RNAs may exhibit various metastable partial folding structures containing many swinging double-strand branches. Additionally, the coupling of some proteins with RNAs may also modify the shape and effective size of the RNAs. In these cases, the RNA model can be modified to include slightly smaller and more rigid particles than that assumed in the presented model. However, the approachable distance among the centers of such particles are expected to be qualitatively similar to those among large and soft particles in simulations with an appropriate range of $k_B T$. Therefore, the results are expected to remain unchanged even after such modifications to the model.

In this study, the physicochemical and biochemical origins of effective interactions among the representative components of condensates in nuclear speckles were not clarified. The electrostatic interactions among the molecules seemed to be one of the strong candidates for the origin of these effective networks. However, the condensation and dispersion of molecules in nuclear speckles could not be explained only by electrostatic interactions because of the following reasons.

Regarding the electrostatic properties of molecules, the interaction parameters between each pair of particles can be assumed as follows:

The IDRs of SRRM2 contained 642 serine and 468 arginine residues and those of SRSF2 contained 42 serine and 35 arginine residues. Therefore, SC35p was expected to exhibit a negative charge. Conversely, SON was expected to exhibit a positive charge because the serine–arginine-rich IDR contains 87 arginine and 67 serine residues. Therefore, an attractive force between the SC35p and SON particles could be assumed because the electrostatic attractive forces may work in between these particles. Conversely, self-repulsions may be assumed between two SRRM2 particles, two SRSF2 particles, and two SON particles because both particles in each pair have the same charges. Additionally, RNAs are negatively charged polymers. Therefore, repulsive forces were assumed among the RNAs.

Both SRRM2 and SRSF2 have RNA-binding sites [27]. RNA binding through such specific binding sites is generally expected to be stronger than binding through non-specific electrostatic forces. Therefore, although the total charges of SRRM2 and SRSF2 were negative, attractive forces could be assumed between SC35p and RNA (*MALAT1* and pre-mRNA) particles.

Similar to SC35p, SON also contains RNA-binding sites [27,33]. Additionally, the total charge of SON was expected to be positive. Therefore, an attractive force between SON and RNA particles was naturally assumed. However, the strength of the attraction between SON and RNA particles was expected to be at least similar to or larger than that between SON and SC35p because RNAs were expected to have a stronger negative charge than that of SC35p.

As expected previously, the model assuming the attractive force between SON and pre-mRNA cannot reproduce the dispersion of SON in the case of *MALAT1* knock-down (Supplementary Fig. S7). This fact suggests that these components were expected to form both electrostatic interactions and a specific affinity-based interaction network that was stronger than the electrostatic interactions.

Based solely on the present arguments, the chemo-mechanical origins of these interactions cannot be clarified. Therefore, further experimental studies are warranted to elucidate the specific molecular binding sites and manner of protein binding. Further, the influences of protein modifications including serine phosphorylation of SR proteins and the possibility of other interactions should be clarified using other molecules. Moreover, we have only simulated a few droplet-like molecular condensates. Therefore, expanding the proposed model to include more particles for the simulation of all nuclear structural behaviors of nuclear speckles using higher performance computations is a crucial future issue.

Conclusion

Overall, a coarse-grained molecular dynamics model of nuclear speckle was developed, and the interaction network among representative molecules, SRRM2, SON, *MALAT1*, and pre-mRNA, was inferred as follows: SRRM2 exhibited attractive interactions with all other molecules; SRRM2–SON attractive interaction was assumed to be similar or slightly weaker than the SRRM2–pre-mRNA attractive interaction; SRRM2–*MALAT1* attractive interaction was assumed to be slightly weaker than the SRRM2–SON attractive interaction (Figure 6A); and attractive interactions also occurred between SON and *MALAT1*. Simulations of this model reproduced a rich variety of experimentally observed states of the droplet-like condensates of such nuclear body.

Conflict of Interest

The authors declare that they have no conflict of interests.

Author Contributions

S.W., N.S., and A.A. conceived and designed the study; S.W. and A.A. performed the mathematical model construction and simulations; S.W. and A.A. analyzed the data; S.W., N.S., and A.A. wrote the manuscript.

Data Availability

The evidence data generated and/or analyzed during the current study are available from the corresponding author on reasonable request.

Acknowledgments

References

[1] Pederson, T. Dynamics and genome-centricity of interchromatin domains in the nucleus. Nat. Cell Biol. 4, E287–E291 (2002). https://doi.org/10.1038/ncb1202-e287

[2] Mao, Y. S., Zhang, B., Spector, D. L. Biogenesis and function of nuclear bodies. Trends Genet. 27, 295–306 (2011). https://doi.org/10.1016/j.tig.2011.05.006

[3] Matsumori, H., Watanabe, K., Tachiwana, H., Fujita, T., Ito, Y., Tokunaga, M., et al. Ribosomal protein L5 facilitates rDNA-bundled condensate and nucleolar assembly. Life Sci. Alliance 5, lsa.202101045 (2022). https://doi.org/10.26508/lsa.202101045

[4] Saitoh, N., Spahr, C. S., Patterson, S. D., Bubulya, P., Neuwald, A. F., Spector, D. L. Proteomic analysis of interchromatin granule clusters. Mol. Biol. Cell. 15, 3876–3890 (2004). https://doi.org/10.1091/mbc.e04-03-0253

[5] Dopie, J., Sweredoski, M. J., Moradian, A., Belmont, A. S. Tyramide signal amplification mass spectrometry (TSA-MS) ratio identifies nuclear speckle proteins. J. Cell Biol. 219, e201910207 (2020). https://doi.org/10.1083/jcb.201910207

[6] Spector, D. L., Lamond, A. I. Nuclear speckles. Cold Spring Harb. Perspect. Biol. 3, 1–12 (2011). https://doi.org/10.1101/cshperspect.a000646

[7] Smith, K. P., Hall, L. L., Lawrence, J. B. Nuclear hubs built on RNAs and clustered organization of the genome. Curr. Opin. Cell Biol. 64, 67–76 (2020). https://doi.org/10.1016/j.ceb.2020.02.015

[8] Tripathi, V., Ellis, J. D., Shen, Z., Song, D. Y., Pan, Q., Watt, A. T., et al. The nuclear-retained noncoding RNA MALAT1 regulates alternative splicing by modulating SR splicing factor phosphorylation. Mol. Cell 39, 925–938 (2010). https://doi.org/10.1016/j.molcel.2010.08.011

[9] Thiry, M. Behavior of interchromatin granules during the cell cycle. Eur. J. Cell Biol. 68, 14–24 (1995).

[10] Lamond, A. I., Spector, D. L. Nuclear speckles: A model for nuclear organelles. Nat. Rev. Mol. Cell Biol. 4, 605–612 (2003). https://doi.org/10.1038/nrm1172

[11] Hall, L. L., Smith, K. P., Byron, M., Lawrence, J. B. Molecular anatomy of a speckle. Anat. Rec. A Discov. Mol. Cell. Evol. Biol. 288, 664–675 (2006). https://doi.org/10.1002/ar.a.20336

[12] Cajal, S. R. El núcleo de las células piramidales del cerebrohumano y de algunos mamíferos. Trab. Lab. Invest. Biol. 8, 27–62 (1910).

[13] Kim, J., Han, K. Y., Khanna, N., Ha, T., Belmont, A. S. Nuclear speckle fusion via long-range directional motion regulates speckle morphology after transcriptional inhibition. J. Cell Sci. 132, jcs226563 (2019). https://doi.org/10.1242/jcs.226563

[14] Chen, Y., Belmont, A. S. Genome organization around nuclear speckles. Curr. Opin. Genet. Dev. 55, 91–99 (2019). Elsevier Ltd. https://doi.org/10.1016/j.gde.2019.06.008

[15] Ilık, İ. A., Malszycki, M., Lübke, A. K., Schade, C., Meierhofer, D., Aktaş, T. Son and SRRM2 are essential for nuclear speckle formation. eLife 9, 60579 (2020). https://doi.org/10.7554/eLife.60579

[16] Zhang, Q., Kota, K. P., Alam, S. G., Nickerson, J. A., Dickinson, R. B., Lele, T. P. Coordinated dynamics of RNA splicing speckles in the nucleus. J. Cell. Physiol. 231, 1269–1275 (2016). https://doi.org/10.1002/jcp.25224

[17] Johnson, C., Primorac, D., Mckinstry, M., Mcneil, J., Rowe, D., Lawrence, J. B. Tracking COL1A1 RNA in osteogenesis imperfecta: Splice-defective transcripts initiate transport from the gene but are retained within the SC35 Domain. J. Cell Biol. 150, 417–432 (2020). https://doi.org/10.1083/jcb.150.3.417

[18] Wang, K., Wang, L., Wang, J., Chen, S., Shi, M., Cheng, H. Intronless mRNAs transit through nuclear speckles to gain export competence. J. Cell Biol. 217, 3912–3929 (2018). https://doi.org/10.1083/jcb.201801184

[19] Fu, X. D., Maniatis, T. Factor required for mammalian spliceosome assembly is localized to discrete regions in the nucleus. Nature 343, 437–441 (1990). https://doi.org/10.1038/343437a0

[20] Fei, J., Jadaliha, M., Harmon, T. S., Li, I. T. S., Hua, B., Hao, Q., et al. Quantitative analysis of multilayer organization of proteins and RNA in nuclear speckles at super resolution. J. Cell Sci. 130, 4180–4192 (2017). https://doi.org/10.1242/jcs.206854

[21] Sharma, A., Takata, H., Shibahara, K., Bubulya, A., Bubulya, P. A. Son is essential for nuclear speckle organization and cell cycle progression. Mol. Biol. Cell 21, 650–663 (2010). https://doi.org/10.1091/mbc.e09-02-0126

[22] O'Keefe, R. T., Mayeda, A., Sadowski, C. L., Krainer, A. R., Spector, D. L. Disruption of pre-mRNA splicing in vivo results in reorganization of splicing factors. J. Cell Biol. 124, 249–260 (1994). https://doi.org/10.1083/jcb.124.3.249

[23] Feric, M., Vaidya, N., Harmon, T. S., Mitrea, D. M., Zhu, L., Richardson, T. M., et al. Coexisting liquid phases underlie nucleolar subcompartments. Cell 165, 1686–1697 (2016). https://doi.org/10.1016/j.cell.2016.04.047

[24] Yamazaki, T., Yamamoto, T., Yoshino, H., Souquere, S., Nakagawa, S., Pierron, G., et al. Paraspeckles are constructed as block copolymer micelles. EMBO J. 40, e107270 (2021). https://doi.org/10.15252/embj.2020107270

[25] Fu, X. D., Maniatis, T. Isolation of a complementary DNA that encodes the mammalian splicing factor SC35. Science 256, 535–538 (1992). https://doi.org/10.1126/science.1373910

[26] Blencowe, B. J., Baurén, G., Eldridge, A. G., Issner, R., Nickerson, J. A., Rosonina, E., et al. The SRm160/300 splicing coactivator subunits. RNA 6, 111–120 (2000). https://doi.org/10.1017/s1355838200991982

[27] Bateman, A., Martin, M.-J., Orchard, S., Magrane, M., Ahmad, S., Alpi, E., et al. UniProt: The universal protein knowledgebase in 2023. Nucleic Acids Res. 51, D523–D531 (2022). https://doi.org/10.1093/nar/gkac1052

[28] Varadi, M., Anyango, S., Deshpande, M., Nair, S., Natassia, C., Yordanova, G., et al. AlphaFold protein structure database: Massively expanding the structural coverage of protein-sequence space with high-accuracy models. Nucleic Acids Res. 50, D439–D444 (2022). https://doi.org/10.1093/nar/gkab1061

[29] Jumper, J., Evans, R., Pritzel, A., Green, T., Figurnov, M., Ronneberger, O., et al. Highly accurate protein structure prediction with AlphaFold. Nature 596, 583–589 (2021). https://doi.org/10.1038/s41586-021-03819-2

[30] Gao, J., Weiner, J. H. Excluded-volume effects in rubber elasticity. 2. ideal chain assumption. Macromolecules 20, 2525–2531 (1987). https://doi.org/10.1021/ma00176a035

[31] Lander, S., Linton, L. M., Birren, B., Nusbaum, C., Zody, M. C., Baldwin, J., et al. Initial sequencing and analysis of the human genome. Nature 409, 860–921 (2001). https://doi.org/10.1038/35057062

[32] Lin, Y. T., Frömberg, D., Huang, W., Delivani, P., Chacón, M., Tolić, I. M., et al. Pulled polymer loops as a model for the alignment of meiotic chromosomes. Phys. Rev. Lett. 115, 208102 (2015). https://doi.org/10.1103/PhysRevLett.115.208102

[33] Ahn, E. Y., DeKelver, R. C., Lo, M. C., Nguyen, T. A., Matsuura, S., Boyapati, A., et al. SON controls cell-cycle progression by coordinated regulation of RNA splicing. Mol. Cell. 42, 185–198 (2011). https://doi.org/10.1016/j.molcel.2011.03.014